aerospace

MDPI

Article

Correction-Efficiency-Coefficient-Based Trajectory Optimization for Two-Dimensional Trajectory Correction Projectile

Dejian Zhang [1,*], Jian Zhang [1], Zhigang Jiao [1], Qingjie Ni [2] and Qiuping Guo [3]

[1] School of Equipment Engineering, Shenyang Ligong University, Shenyang 110159, China; zbgc421@aliyun.com (J.Z.); 13504975840@163.com (Z.J.)
[2] Liao Shen Industries Group Co., Ltd., Shenyang 110045, China; nq724724@163.com
[3] The Second Army Represent Office, Shenyang 110016, China; wubo_00@126.com
* Correspondence: zhangdj_bq1992@163.com; Tel.: +86-13664179255

Abstract: Based on the lift-to-drag ratio of a two-dimensional trajectory correction projectile, in this paper, a novel correction efficiency coefficient model has been proposed for the trajectory optimization of a two-dimensional trajectory correction projectile, and research on the influence a correction efficiency coefficient has on the flight parameters of correction trajectory is carried out. A series of results are obtained through theoretical analysis and simulation calculations, indicating that, the smaller the value of the correction efficiency coefficient is, the stronger the correction ability of the projectile reserves. The trajectory and canard geometry of the correction section of the two-dimensional trajectory correction projectile are optimized by the Gauss pseudo-spectral method and correction efficiency coefficient, and, after taking the correction efficiency coefficient into account, the projectile can accurately hit the target and effectively eliminate the swing phenomenon of the projectile's lateral trajectory. Meanwhile, a stable roll control command is obtained. When the diameter aspect ratio of the canard is 0.4, both the flight state quantity of the optimized projectile and the roll control command are more stable, and, when the canard shape is trapezoidal, the correction efficiency coefficient is smaller, the result of trajectory optimization is more stable, and the stability of the output roll control command is better. The research results of this paper can provide certain references for both the designs of the two-dimensional trajectory correction projectile's trajectory and the canard geometry.

Keywords: trajectory optimization; correction efficiency coefficient; canard geometry

Citation: Zhang, D.; Zhang, J.; Jiao, Z.; Ni, Q.; Guo, Q. Correction-Efficiency-Coefficient-Based Trajectory Optimization for Two-Dimensional Trajectory Correction Projectile. *Aerospace* **2022**, *9*, 149. https://doi.org/10.3390/aerospace9030149

Academic Editors: Judith Rosenow and Dario Modenini

Received: 29 December 2021
Accepted: 3 March 2022
Published: 8 March 2022

1. Introduction

The two-dimensional trajectory correction projectile is a guided projectile whose fuze is changed from a conventional projectile to a two-dimensional correction component to achieve the precise suppression of the target. It is one of the most effective ways to intellectualize conventional projectiles with lower cost, less technical complexity, and higher precision. The development of the two-dimensional trajectory correction projectile aims to cut down the consumption of ammunition, relieve the burden of supplying, reduce collateral damage, and, therefore, accelerate the battle. The two-dimensional trajectory correction projectile can be divided into two parts: the projectile body and the correction component. The correction component is composed of a fuze and two pairs of canards, as shown in Figure 1 [1]. Among the two pairs of canards, one pair are the differential canards, and the other are the steering canards, all of which are separated from the fuze. The fuze rotates with and the canards counter-rotate with the projectile body. The control force and control moment that are provided by the differential canard can correct the projectile's trajectory both horizontally and longitudinally. The trajectory of a two-dimensional trajectory correction projectile can be divided into two sections, namely the uncontrolled section and the correction section, and the optimizing of the latter can directly affect the

shooting accuracy and damage effect of the projectile. Hence, it is meaningful to establish a reasonable optimization model and determine the optimal trajectory of the projectile in the correction section [2].

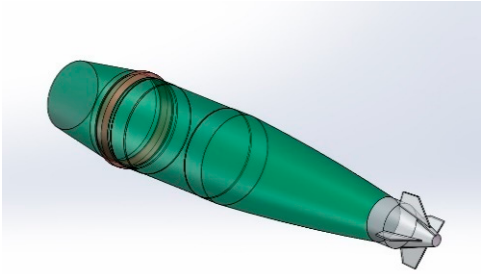

Figure 1. Schematic diagram of two-dimensional trajectory correction projectile.

The equations of motion for a projectile are the basis of trajectory optimization. Compared with conventional projectiles, the rolling of the forward body of a two-dimensional trajectory correction projectile is increased, and its trajectory model is somewhat different from the conventional ones. Costello M [3] first established a seven-degree-of-freedom projectile trajectory dynamic model to calculate the trajectory of dual-spin projectiles. Wernert [4] established a seven-degree-of-freedom non-linear flight dynamics equation of a dual-spin projectile equipped with CCF and studied the balance and maneuverability of the projectile. Sijiang Chang [5] deduced the equation of motion of the point mass and the equation of motion around the point mass of the dual-spin projectile's seven-degree-of-freedom rigid body and ran the simulation analysis on the trajectory's characteristics of the dual-spin projectiles with fixed canards.

Currently, the research on trajectory optimization focuses mainly on two aspects: one is the research on optimization algorithms, and the other is the optimization of trajectory indicators. In the former case, there are algorithms, such as the direct shooting method [6], pseudo-spectral method [7], and maximum/minimum principle [8], etc., and, in recent years, some intelligent algorithms have been developed, such as the genetic algorithm (GA) [9], particle swarm optimization (PSO) [10], and neural network algorithm (ANN) [11], all of which have their own pros and cons and can be used to solve trajectory optimization problems in different situations. In the latter, some researchers applied the above optimization methods in regard to the research of the guidance section of a ballistic correction projectile, the control section of a multistage rocket projectile, the gliding section of a gliding guidance projectile, and the structure of the spoiler of a ballistic correction projectile. Costello M [12] took the falling velocity as the constraint and the maximum range as the objective function to optimize the trajectory of the guided projectile. Based on the Gaussian pseudo-spectral method (GPM), Chaoyue Liu [13] et al. proposed a multistage trajectory optimization method to optimize the multistage trajectory of a two-stage booster rocket and obtain the feasible optimal trajectory; Qi Chen [14] et al. optimized the multiphase trajectory of a gliding guided projectile by considering continuous and discrete variables; Qiuping Xu [15] et al. optimized the gliding trajectory of a gliding guided projectile by using the compose efficiency factor model; Bradley T. Burchett [16] et al. designed a trajectory prediction method that can accurately and quickly predict the trajectory of a rotating stable projectile with high launch height and transonic speed; based on the maximum/minimum principle, J Yao [17] et al. deduced the trajectory correction optimal control strategy with minimum undershoot and minimum energy as an objective function. Yu Wu [18] et al. proposed a hybrid PSO–GPM algorithm to deal with the reentry trajectory optimization problem. The reasonable reentry trajectory optimization model was obtained, and the flight safety level was improved. Guillaume Arnoult [19] et al. combined the Kriging with ANN to optimize the structural parameters of the spoiler and optimize the lateral distance of the trajectory correction projectile. In addition, some researchers have proposed different optimization algorithms and optimized the trajectory of trajectory

correction projectiles, missiles, gliders, autonomous driving vehicles, and mechanical arms. Wei Zhou [20] et al. adopted parametric optimization methods to optimize the grid structure used in the calculation of aerodynamic parameters of trajectory correction projectiles; Zhenbo Wang [21] et al. optimized the flight trajectory of a hypersonic glider based on the convex optimization method; Kwon hyuck Hoon [22] et al. used second-order cone programming (SOCP) to solve the midcourse trajectory optimization problem of the boost gliding missile. By comparing with other optimization methods, the superiority of SOCP is verified. Dhruv Laad [23] et al. studied a Floquet index and eigenvector estimation technology based on the time-domain discretization of Floquet eigenvectors BVP and integrated the method into Fourier pseudo-spectrum optimization to optimize the gliding trajectory of the glider. Elsis. M optimized the trajectory of autopilot and a mechanical arm based on the improved multi-tracking optimization algorithm [24], SSDA [25], and improved grey wolf optimization algorithm [26].

To sum up, previous research results on the optimization design of trajectory mostly focused on weapons platforms with a long range, smooth flight trajectory, and long flight time, such as missiles, gliding guided projectiles, and gliding aircraft, and obtained better results. The research object of this paper is the fixed canard dual-spin projectile, which has complex flight attitude, short flight time, and fast descent speed, which make it necessary to design a reasonable objective function to optimize the flight trajectory. The main contribution of the research results of this paper is to put forward a new concept of a correction efficiency coefficient (CEC) that can be used as the objective function to control the two-dimensional trajectory correction projectile to hit the target, and, at the same time, in the geometric structure design of canards. The practical significance of a CEC is that it can not only effectively describe the correction capability of a two-dimensional trajectory correction projectile but also reflect the influence of canard geometry on trajectory correction capability, which has not yet been mentioned in the previously published research results. Therefore, the use of a CEC can provide an alternative method for the trajectory optimization and geometric structure design of a two-dimensional trajectory correction projectile. Based on the optimization of the CEC, we can obtain a stable and reasonable flight trajectory and the optimal canard geometry, which provides a reference for improving the performance of the projectile and engineering application.

Based on the lift-to-drag ratio, a correction efficiency coefficient (CEC) model for the trajectory optimization of two-dimensional trajectory correction projectiles is established, and the influence of the CEC on the trajectory's characteristics of two-dimensional trajectory correction projectiles is studied. Taking the CEC and impact point deviation as optimization objects, different forms of cost functions are established, GPM is used to optimize the trajectory of the two-dimensional trajectory correction projectile in the correction section, and then a smooth trajectory and stable roll control command are obtained. Through optimized calculations for different targets, the feasibility and effectiveness of the CEC model are verified. Finally, the optimization calculation of two-dimensional trajectory correction projectiles with different canard structural parameters is carried out in combination with the CEC, the influence of structural parameters on the optimization results is discussed, and a set of optimal structural parameters is obtained.

The present paper is organized as follows: the motion equation and CEC model of the projectile are established in Section 2; the influence of the CEC on ballistic characteristics is analyzed in Section 3; the optimization of the trajectory of the two-dimensional trajectory correction projectile based on the CEC is in Section 4; the optimized design of the canard mechanism based on the CEC is in Section 5, and the summary is in Section 6.

2. Correction Efficiency Coefficient

2.1. Equation of Motion

This section uses the rigid-body trajectory model established by S. Chang to describe the trajectory and motion attitude of the two-dimensional trajectory correction projectile [5]. However, in a practical flight, it is difficult to obtain all the trajectory parameters that meet

the computational demands of a rigid body trajectory, and, in the combat mission performing process of the two-dimensional trajectory correction projectile, the main focus is on the correction of the flight trajectory. Hence, it is necessary to simplify the trajectory equation of the seven-degree-of-freedom rigid body to meet the needs of trajectory optimization.

Assumptions for simplification:

(1) The principal axes of inertia of the forward and aft bodies are parallel to that of the combination.
(2) The force and moment are uniformly applied to the whole projectile;
(3) The aerodynamic coupling of forces and moments acted on the projectile is neglected.
(4) Magnus force and Coriolis inertial force are ignored;
(5) The influence of wind is not considered

In trajectory-fixed coordinate system, the simplified equations of motion are [27]:

$$\begin{cases} m\dot{v} = -F_X - mg\sin\theta\cos\psi \\ mv\cos\psi\dot{\theta} = F_Y - mg\cos\theta \\ mv\dot{\psi} = F_Z + mg\sin\theta\sin\psi \\ \dot{x} = v\cos\theta\cos\psi \\ \dot{y} = v\sin\theta\cos\psi \\ \dot{z} = v\sin\psi \end{cases} \tag{1}$$

where v is the speed; θ is the slope angle of trajectory; ψ is the deflection angle; m is the mass; g is the gravitational acceleration; the x, y, and z coordinates define the position of the projectile in the three-dimensional coordinate system; F_X, F_Y, and F_Z is the join force on the projectile.

In the flight process, the join force of the two-dimensional trajectory correction projectile consists of two parts: the aerodynamic force generated by the projectile and the control force provided by the canard. The main aerodynamic forces of projectile are drag and lift; the derivation process is as follows.

In the coordinate system of projectile axes, the expressions of projectile's drag and lift are as follows:

$$\begin{cases} R_X = -QSc_{x_0}(1 + k\delta^2) \\ R_Y = QSc_y \end{cases} \tag{2}$$

where Q is the dynamic pressure, $Q = 0.5\rho v^2$; S is the reference area; c_{x_0} is drag force coefficients; c_y is lift force coefficients.

Equation (2) is expressed in the trajectory-fixed coordinate system as follows:

$$\begin{cases} R_{X_2} = -QSc_{x_0}(1 + k\delta^2) \\ R_{Y_2} = QSc_y\cos\beta\sin\alpha \\ R_{Z_2} = QSc_y\sin\beta \end{cases} \tag{3}$$

where δ is the angle of attack, $\delta = \sqrt{\alpha^2 + \beta^2}$; α and β are the pitch and transverse components of angle of attack.

The canard mainly provides the control force required for trajectory correction, and its expression is:

$$\begin{cases} R_{CX} = 0 \\ R_{CY} = QSc_{N_\delta}\delta_z\cos\gamma_f \\ R_{CZ} = QSc_{N_\delta}\delta_z\sin\gamma_f \end{cases} \tag{4}$$

where c_{N_δ} is control force coefficient for canards; δ_z is the deflection angles; γ_f is the roll angles of forward body.

Equation (4) is expressed in the trajectory-fixed coordinate system as follows:

$$\begin{cases} R_{CX_2} = -QSc_{N_\delta}\delta_z(\cos\gamma_f\sin\alpha + \sin\gamma_f\cos\alpha\sin\beta) \\ R_{CY_2} = QSc_{N_\delta}\delta_z(\cos\alpha\cos\gamma_f - \sin\alpha\sin\beta\sin\gamma_f) \\ R_{CZ_2} = QSc_{N_\delta}\delta_z\cos\beta\sin\gamma_f \end{cases} \tag{5}$$

Add Equations (3) and (5) to get the expression of join force in the flight process of the two-dimensional trajectory correction projectile:

$$\begin{cases} F_X = -QS[c_{x_0}(1+k\delta^2) + c_{N_\delta}\delta_z(\cos\gamma_f \sin\alpha + \sin\gamma_f \cos\alpha \sin\beta)] \\ F_Y = QS[c_y \cos\beta \sin\alpha + c_{N_\delta}\delta_z(\cos\alpha \cos\gamma_f - \sin\alpha \sin\beta \sin\gamma_f)] \\ F_Z = QS(c_y \sin\beta + c_{N_\delta}\delta_z \cos\beta \sin\gamma_f) \end{cases} \tag{6}$$

If α and β are small quantities, then Equation (6) is simplified to:

$$\begin{cases} F_X = -QSc_{x_0}(1+k\delta^2) - QSc_{N\delta}\delta_z(\alpha \cos\gamma_f + \beta \sin\gamma_f) \\ F_Y = QSc_y\alpha + QSc_{N_\delta}\delta_z \cos\gamma_f \\ F_Z = QSc_y\beta + QSc_{N_\delta}\delta_z \sin\gamma_f \end{cases} \tag{7}$$

According to the two-dimensional trajectory correction projectile angular motion equation, the moment equilibrium condition is derived, which is used to establish the CEC model later. Under the control of canards, the motion equation of the two-dimensional trajectory correction projectile linear angle of attack is:

$$\begin{aligned} &\boldsymbol{\Delta}'' + (H - \mathrm{i}P)\boldsymbol{\Delta}' - (M + \mathrm{i}PT)\boldsymbol{\Delta} = \widetilde{C} \\ &H = k_{zz} + b_y - b_x - \tfrac{2g\sin\theta}{v^2} \\ &P = \tfrac{(C_f\omega_{fx} + C_a\omega_{ax})}{Av} \\ &M = k_z = \tfrac{\rho SLc_{M_\alpha}}{2A} \\ &T = b_y - k_y\tfrac{\omega_{ax}}{Pv} \\ &\widetilde{C} = \left[\left(b_x + \tfrac{g\sin\theta}{v^2} + \mathrm{i}P - k_{zz} - \mathrm{i}\gamma'_f\right)b_c\delta_z + k_c\delta_z\right]e^{\mathrm{i}\gamma_f} \end{aligned} \tag{8}$$

where $\boldsymbol{\Delta}$ is the plural form of angle of attack; b_x is the plural form of air drag; b_y is the plural form of lift; b_c is the plural form of control force coefficient for canards; k_z is the plural form of static moment; k_{zz} is the plural form of pitch damping moment; k_c is the plural form of control moment for canards, the expressions, as shown in Table 1; c_{M_α} is the static moment coefficient; $c_{M_{zz}}$ is the pitch damping moment coefficient; c_{M_δ} is the control force coefficient for canards; A is the equatorial moment of inertia; ρ is the air density; L is the reference length; C_f is the moment of inertia of the forward body; C_a is the moment of inertia of the aft body; ω_{fx} is the rotational angular velocity of the forward body; ω_{ax} is the rotational angular velocity of the aft body.

Table 1. The plural form of aerodynamic force.

Aerodynamic Force	Expressions
Drag	$b_x = \rho Sc_x/(2m)$
Lift	$b_y = \rho Sc_y/(2m)$
Control force for canards	$b_c = \rho Sc_{N_\delta}/(2m)$
Static moment	$k_z = \rho SLc_{M_\alpha}/(2A)$
Pitch damping moment	$k_{zz} = \rho SLDc_{M_{zz}}/(2A)$
Control moment for canards	$k_c = \rho SLc_{M_\delta}/(2A)$

When the projectile flight in a stable state, $\boldsymbol{\Delta}'' = 0$, $\boldsymbol{\Delta}' = 0$, and then:

$$\boldsymbol{\Delta} = -\frac{1}{M + \mathrm{i}PT}\left[\left(b_x + \frac{g\sin\theta}{v^2} + \mathrm{i}P - k_{zz} - \mathrm{i}\gamma'_f\right)b_c\delta_z + k_c\delta_z\right]e^{\mathrm{i}\gamma_f} \tag{9}$$

Ignore the smaller forces and moments in Equation (9), and obtain the balance condition of the two-dimensional trajectory correction, which is:

$$\boldsymbol{\Delta} = -\frac{1}{k_z}k_c\delta_z e^{\mathrm{i}\gamma_f} \tag{10}$$

Substituting k_c and k_z into Equation (10), we get:

$$\boldsymbol{\Delta} = -\frac{c_{M_\delta}}{c_{M_\alpha}}\delta_z e^{i\gamma_f} \tag{11}$$

According to Euler's formula:

$$\alpha + i\beta = -\frac{c_{M_\delta}}{c_{M_\alpha}}\delta_z(\cos\gamma_f + i\sin\gamma_f) \tag{12}$$

The pitch components angle of attack and transverse components angle of attack are:

$$\begin{cases} \alpha = -\frac{c_{M_\delta}}{c_{M_\alpha}}\delta_z\cos\gamma_f \\ \beta = -\frac{c_{M_\delta}}{c_{M_\alpha}}\delta_z\sin\gamma_f \end{cases} \tag{13}$$

Let $c_{\alpha\delta} = -\frac{c_{M_\delta}}{c_{M_\alpha}}$; then, Equation (13) is expressed as:

$$\begin{cases} \alpha = c_{\alpha\delta}\delta_z\cos\gamma_f \\ \beta = c_{\alpha\delta}\delta_z\sin\gamma_f \end{cases} \tag{14}$$

Substituting Equation (14) in Equation (7), the aerodynamic model is expressed as follows:

$$\begin{cases} F_X = -QS[c_{x_0} + 2(c_{x_0}kc_{\alpha\delta}^2 + c_{N_\delta}c_{\alpha\delta})\delta_z^2] \\ F_Y = QS(c_yc_{\alpha\delta} + c_{N_\delta})\delta_z\cos\gamma_f \\ F_Z = QS(c_yc_{\alpha\delta} + c_{N_\delta})\delta_z\sin\gamma_f \end{cases} \tag{15}$$

2.2. Correction Efficiency Coefficient

The lift-to-drag ratio of a two-dimensional trajectory correction projectile refers to the ratio of the lift and drag of the projectile at the same angle of attack under the control of the canards, which is an important parameter for evaluating the aerodynamic characteristics and aerodynamic efficiency of the two-dimensional trajectory correction projectile.

Suppose the ratio of lift to drag of the two-dimensional trajectory correction projectile K_{TY} is:

$$K_{TY} = \frac{F_Y}{F_X} = \frac{K_F\delta_{zy}}{K_B + K_A\delta_{zy}^2} \tag{16}$$

In the same way, the ratio of lateral force to drag is:

$$K_{TZ} = \frac{K_F\delta_{zz}}{K_B + K_A\delta_{zz}^2} \tag{17}$$

where $K_F = c_yc_{\alpha\delta} + c_{N\delta}$; $K_A = 2(c_{x_0}kc_{\alpha\delta}^2 + c_{N\delta}c_{\alpha\delta})$; $K_B = c_{x_0}$; both are functions of Mach number; δ_{zy} is the vertical equivalent deflection angle, $\delta_{zy} = \delta_z\cos\gamma_f$; δ_{zz} is the lateral equivalent deflection angle, $\delta_{zz} = \delta_z\sin\gamma_f$.

To transform Equations (16) and (17):

$$K_{TY} = \frac{K_F}{K_A\delta_{zy} + \frac{K_B}{\delta_{zy}}} \tag{18}$$

$$K_{TZ} = \frac{K_F}{K_A\delta_{zz} + \frac{K_B}{\delta_{zz}}} \tag{19}$$

As shown in Equation (18), the denominator is the Hook function; if $\delta_{zy} = \hat{\delta}_{zy} = \sqrt{K_B/K_A}$, the denominator has a minimum $2\sqrt{K_AK_B}$, and then $K_{TY\max} = K_F/2\sqrt{K_AK_B}$; in this case, the canard produces positive lift, which is beneficial to extended range of the two-dimensional trajectory correction projectile. If $\delta_{zy} < 0$, then $\hat{\delta}_{zymin} = -\sqrt{K_B/K_A}$ and

$K_{TY\min} = -(K_F/2\sqrt{K_A K_B})$, in this case resulting in negative lift that is not conducive to extended range.

In the same way, if $\delta_{zz} > 0$, then $\delta_{zz} = \hat{\delta}_{zz\max} = \sqrt{K_B/K_A}$; in this case, the canard produces positive lateral force, which is beneficial to extended lateral distance. If $\delta_{zz} < 0$, then $\hat{\delta}_{zz\min} = -\sqrt{K_B/K_A}$, in this case, which is not conducive to extended lateral distance.

The correction efficiency coefficient (CEC) ξ is the ratio of the lift to drag of the two-dimensional trajectory correction projectile to the maximum value of the lift-to-drag ratio, as shown in Equation (17). Decompose CEC into vertical correction efficiency coefficient and lateral correction efficiency coefficient, as shown in Equations (22) and (23).

Here, we define the sign function as follows:

$$\operatorname{sign}(x) = \begin{cases} 1 & x \le 0 \\ -1 & x < 0 \end{cases} \tag{20}$$

$$\xi = \operatorname{sign}(\delta_z)\frac{2\sqrt{K_A K_B}\delta_z}{K_B + K_A\delta_z^2} \tag{21}$$

Vertical correction efficiency coefficient (VCEC) ξ_Y is

$$\xi_Y = \operatorname{sign}(\delta_{zy})\frac{2\sqrt{K_A K_B}\delta_{zy}}{K_B + K_A\delta_{zy}^2} \tag{22}$$

Lateral correction efficiency coefficient (LCEC) ξ_Z is

$$\xi_Z = \operatorname{sign}(\delta_{zz})\frac{2\sqrt{K_A K_B}\delta_{zz}}{K_B + K_A\delta_{zz}^2} \tag{23}$$

The CEC is related to the Mach number and canard's deflection angle of the two-dimensional trajectory correction projectile, as shown in Figure 2. Under the same Mach number, increasing $|\delta_z|$ increases the absolute value of CEC. If $\delta_z > 0$, CEC > 0 canard provides positive correction effect; if $\delta_z < 0$, CEC < 0, canard provides negative correction effect; if $\delta_z = 0$, CEC = 0, the projectile has no correction effect. Under the same deflection angle, increasing the Mach number increases the absolute value of CEC. Hence, the correction control of the projectile's trajectory can be realized by changing the value of CEC.

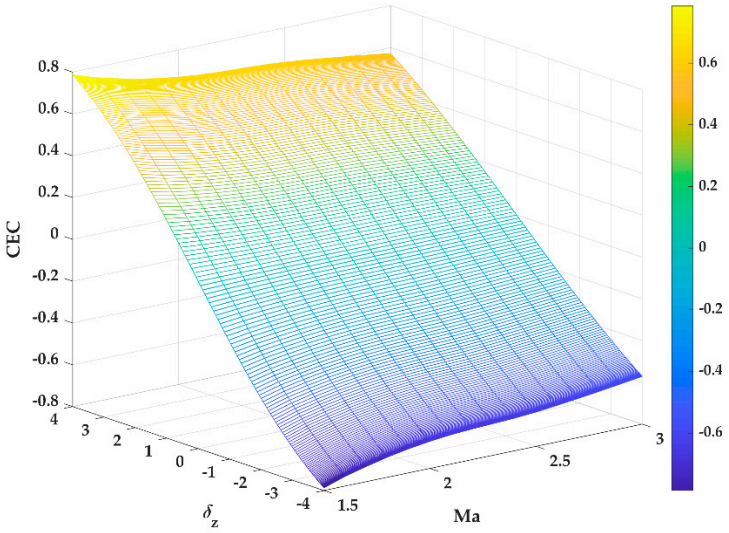

Figure 2. Relationship between CEC, deflection angle, and Mach.

3. Trajectory Characteristics Based on CEC

Solving Equations (22) and (23), the canard deflection angles expressed in CEC are:

$$\delta_{zy} = \frac{\sqrt{K_B}(1 \pm \sqrt{1-\xi_Y^2})}{\sqrt{K_A}\xi_Y} \tag{24}$$

$$\delta_{zz} = \frac{\sqrt{K_B}(1 \pm \sqrt{1-\xi_Z^2})}{\sqrt{K_A}\xi_Z} \tag{25}$$

When $-1 < \xi < 1$, there are two canard deflection angles with CEC (i.e., δ_{z1}, δ_{z2} ($0 < \delta_{z1} < \hat{\delta}_z < \delta_{z2}$)). When ξ goes smaller, the δ_{z1} decreases and δ_{z2} increases. Considering the limitation of the canard deflection angle of the modified mechanism, the larger equivalent canard deflection angle is discarded and the smaller equivalent canard deflection angle is adopted.

$$\delta_{zy} = \frac{\sqrt{K_B}(1 - \sqrt{1-\xi_Y^2})}{\sqrt{K_A}\xi_Y} \tag{26}$$

$$\delta_{zz} = \frac{\sqrt{K_B}(1 - \sqrt{1-\xi_Z^2})}{\sqrt{K_A}\xi_Z} \tag{27}$$

Substituting Equations (26) and (27) into the Equation (1), several sets of constant VCEC and LCEC are selected for simulation calculations to analyze the influence of the CEC on the trajectory characteristics. The initial parameters are shown in Table 2, and the results are shown in Figure 3.

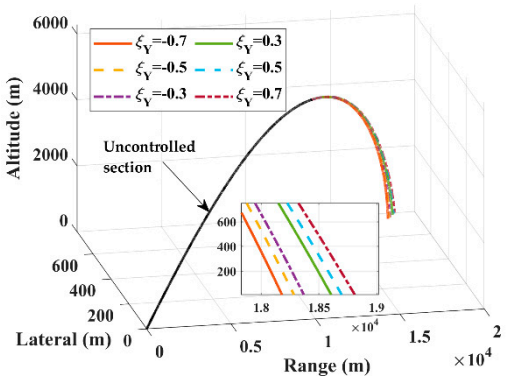

(**a**) Trajectory vs. VCEC

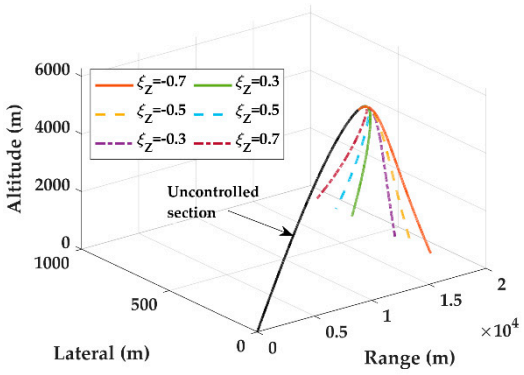

(**b**) Trajectory vs. LCEC

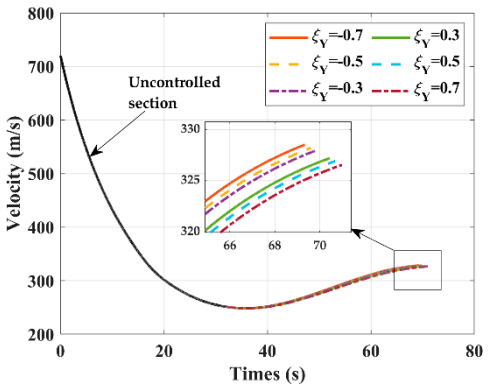

(**c**) Velocity vs. VCEC

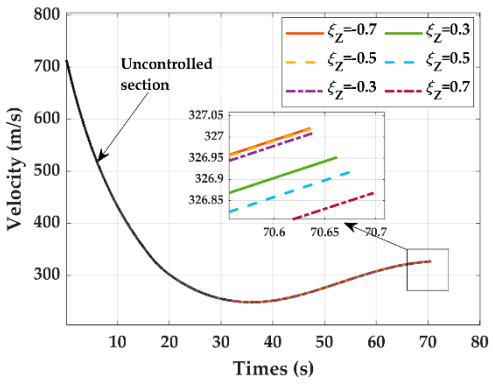

(**d**) Velocity vs. LCEC

Figure 3. *Cont.*

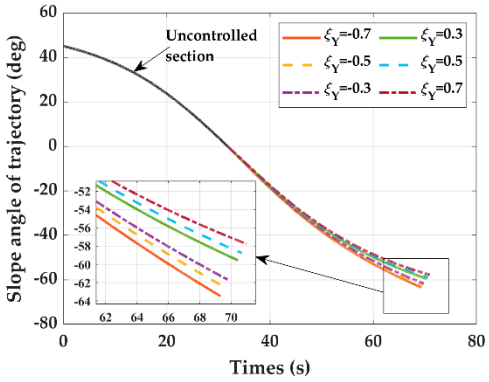

(**e**) Slope angle of trajectory vs. VCEC

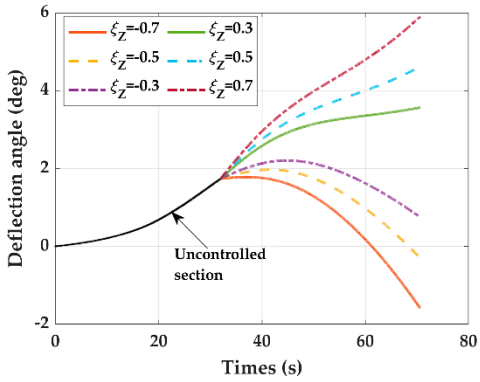

(**f**) Deflection angle vs. LCEC

Figure 3. Trajectory parameter profiles with different CECs.

Table 2. Projectile parameters and initial conditions.

Parameters of Projectile	Values
Mass m, kg	22
Reference area S, m^2	1.17×10^{-2}
Reference length L, m	0.75
Moment of inertia of the forward body C_f	4.5×10^{-2}
Moment of inertia of the aft body C_a	2.25×10^{-3}
Initial velocity v_0, m/s	720
Angle of departure θ_0, deg	45
Start control time t, s	32

(1) VCEC and LCEC can reflect the changing law of the roll angle, as shown in Equation (28).

$$\gamma_f = \arctan\left(\frac{\delta_{zz}}{\delta_{zy}}\right) = \arctan\left[\frac{\xi_Y\left(1-\sqrt{1-\xi_Z^2}\right)}{\xi_Z\left(1-\sqrt{1-\xi_Y^2}\right)}\right] \tag{28}$$

(2) The effect of CEC on impact point

The time derivative of the fourth and sixth terms in Equation (1) are

$$\begin{cases} \ddot{x} = \dot{v}\cos\theta\cos\psi - v\sin\theta\cos\psi\cdot\dot{\theta} - v\cos\theta\sin\psi\cdot\dot{\psi} \\ \ddot{z} = \dot{v}\sin\psi + v\cos\psi\cdot\dot{\psi} \end{cases} \tag{29}$$

Substituting Equations (26) and (27) into Equation (29) and integrating them, the relationship between the range and lateral distance and VCEC and LCEC is obtained. As shown in Equation (30), the change rule of the range and lateral distance is jointly affected by VCEC and LCEC.

$$\begin{cases} x = \iint\left(-\frac{QSK_B\cos\theta\cos\psi}{m}\left(1+\left(\frac{\left(1-\sqrt{1-\xi_Y^2}\right)^2}{\xi_Y^2}+\frac{\left(1-\sqrt{1-\xi_Z^2}\right)^2}{\xi_Z^2}\right)\right) - \frac{QSK_F\sin\theta}{m}\frac{\sqrt{K_B}\left(1-\sqrt{1-\xi_Y^2}\right)}{\sqrt{K_A}\xi_Y} \right. \\ \qquad \left. - \frac{QSK_F\cos\theta\sin\psi}{m}\frac{\sqrt{K_B}\left(1-\sqrt{1-\xi_Z^2}\right)}{\sqrt{K_A}\xi_Z}\right)dt \\ z = \iint\left(-\frac{QSK_B\sin\psi}{m}\left(1+\left(\frac{\left(1-\sqrt{1-\xi_Y^2}\right)^2}{\xi_Y^2}+\frac{\left(1-\sqrt{1-\xi_Z^2}\right)^2}{\xi_Z^2}\right)\right) + \frac{QSK_F\cos\psi}{m}\frac{\sqrt{K_B}\left(1-\sqrt{1-\xi_Z^2}\right)}{\sqrt{K_A}\xi_Z}\right)dt \end{cases} \tag{30}$$

The range is sensitive to the VCEC, as shown in Figure 3a, with the increase in ξ_Y, the longer the range of the projectile is. The lateral distance is sensitive to the LCEC, as shown in Figure 3b. If $\xi_Z > 0$, the trajectory is corrected to the left. If $\xi_Z < 0$, the trajectory is corrected to the right, and, with the increase in ξ_Z, the lateral distance of the projectile becomes larger.

Since the two-dimensional trajectory correction projectile adopts a correction strategy that sets a shooting range that is further than the position of the target but finally obtains the precise hit by adjusting the trajectory with the correction component, smaller VCEC and LCEC are more conducive to provide the effect of trajectory correction.

(3) The effect of CEC on velocity

In a certain flight state, the size of the rate of change of the speed of the projectile is affected by both VCEC and LCEC, as shown in Equation (31).

$$m\dot{v} = -QSK_B\left[1 + \left(\frac{(1-\sqrt{1-\xi_Y^2})^2}{\xi_Y^2} + \frac{(1-\sqrt{1-\xi_Z^2})^2}{\xi_Z^2}\right)\right] - mg\sin\theta\cos\psi \tag{31}$$

The velocity of projectile is mainly affected by VCEC and has little sensitivity to LCEC, as shown in Figure 3c,d. With the decrease in ξ_Y, both the flight and falling velocities of the projectile increase. Hence, a smaller VCEC provides the two-dimensional trajectory correction projectile with less consumption, higher storage of the projectile's speed during the flight, and greater falling speed when the projectile hits the target.

(4) The effect of CEC on slope angle of trajectory

$$mv\cos\psi\dot{\theta} = QSK_F\frac{\sqrt{K_B}(1-\sqrt{1-\xi_Y^2})}{\sqrt{K_A}\xi_Y} - mg\cos\theta \tag{32}$$

The law of slope angle of trajectory is only related to VCEC, as shown in Equation (32) and Figure 3e. When $\xi_Y < 0$, if, $\dot{\theta} < 0$, $\dot{\theta}$ declines with the decrease in ξ_Y; when $\xi_Y > 0$, if $\dot{\theta} < 0$, $\dot{\theta}$ grows with the decrease in ξ_Y; if $\dot{\theta} > 0$, $\dot{\theta}$ becomes smaller with the decrease in ξ_Y. Hence, a smaller VCEC can increase the speed of the projectile and make the projectile hit the target with a larger angle of impact.

(5) The effect of CEC on deflection angle

$$mv\dot{\psi} = QSK_F\frac{\sqrt{K_B}(1-\sqrt{1-\xi_Z^2})}{\sqrt{K_A}\xi_Z} + mg\sin\theta\sin\psi \tag{33}$$

The law of deflection angle is only related to LCEC, as shown in Equation (33) and Figure 3f. When $\xi_Z < 0$, ψ shifts to the left (viewed from the tail of the projectile); if $\dot{\psi} < 0$, $\dot{\psi}$ declines with the decrease in LCEC; when $\xi_Z > 0$, ψ shifts to the left (viewed from the tail of the projectile); if $\dot{\psi} < 0$, $\dot{\psi}$ grows with the decrease in LCEC; if $\dot{\psi} > 0$, $\dot{\psi}$ becomes smaller with the decrease in LCEC. Hence, a smaller LCEC can amplify the rate of increase, thereby increasing the final value of the trajectory deflection angle.

In summary, when the two-dimensional trajectory correction projectile performs trajectory correction, smaller VCEC and LCEC can reduce the speed consumption during the trajectory correction process so that the projectile can hit the target with a larger falling speed and angle. At the same time, the smaller VCEC and LCEC also meet the demands of the two-dimensional trajectory correction projectile's correction strategy.

4. CEC-Based Trajectory Optimization

After the analysis in the previous section, a smaller CEC is conducive to the trajectory optimization calculation of the two-dimensional trajectory correction projectile. In this section, we will establish three different types of cost functions based on the impact point deviation and CEC and use GPM to calculate the trajectory optimization of a two-dimensional trajectory correction projectile and study the influence of CEC on the trajectory of a two-dimensional trajectory correction projectile.

(1) Mayer functions

The Mayer function takes the deviation of the two-dimensional trajectory correction projectile as the cost function and minimizes the deviation of the projectile after optimization, as shown in Equation (34).

$$J_1 = \frac{1}{2}(\Delta x^2 + \Delta z^2) \tag{34}$$

(2) Lagrange functions

The Lagrange function takes the optimized CEC as the cost function to optimize the trajectory of the two-dimensional trajectory correction projectile, as shown in Equation (35).

$$J_2 = \frac{1}{2}\int_{t_0}^{t_f} \xi_{Ky}^2 + \xi_{Kz}^2 dt \tag{35}$$

(3) Composite function

The composite function is the addition of the Lagrange function and the Mayer function, which describes that the optimized trajectory meets the minimum impact point deviation while minimizing the CEC, as shown in Equation (36).

$$J_3 = \frac{1}{2}(\Delta x^2 + \Delta z^2) + \frac{1}{2}\int_{t_0}^{t_f} \xi_{Ky}^2 + \xi_{Kz}^2 dt \tag{36}$$

where Δx and Δz are the impact point deviation, $\Delta x = x(t_f) - x_f$, $\Delta z = z(t_f) - z_f$, x_f and z_f are the targets, t_f is the terminal time. The parameter constraints are shown in Table 3.

Table 3. Parameters of constraints.

Parameters	Values
v_f	free
θ_f	free
ψ_f	free
$(x(t_f), z(t_f))$	free
(x_f, z_f)	(18,000, 500)

4.1. Gauss Pseudo-Spectral Method

The Gauss pseudo-spectral method (GPM) is a fast and real-time optimization method that was first proposed by David Benson [28] when trying to improve the estimation accuracy of the Legendre pseudo-spectral method. The main idea is to discretize the continuous Bolza problem of optimal control into a nonlinear programming problem (NLP), and then use a numerical method to solve the NLP problem and obtain its optimal solution. In this study, the GPOPS [29] software package and SNOPT [30] software package were used to discretize and solve the trajectory optimization problem of the two-dimensional trajectory correction projectile. The parameter settings are shown in Table 4, and the solution process is shown in Figure 4.

Table 4. Main setting parameters.

Description	Definition in GPOPS	Values
Mesh refinement tolerance	Setup.mesh.tolerance	10^{-4}
Number of mesh refinement iterations	Setup.mesh.iteration	25
Minimum number of allowed collocation points in a mesh interval	Setup.nodesPerInterval.min	4
Maximum number of allowed collocation points in a mesh interval	Setup.nodesPerInterval.max	12
Automatic scaling	Setup.autoscale	on
Derivative computation	Setup.derivatives	finite-difference

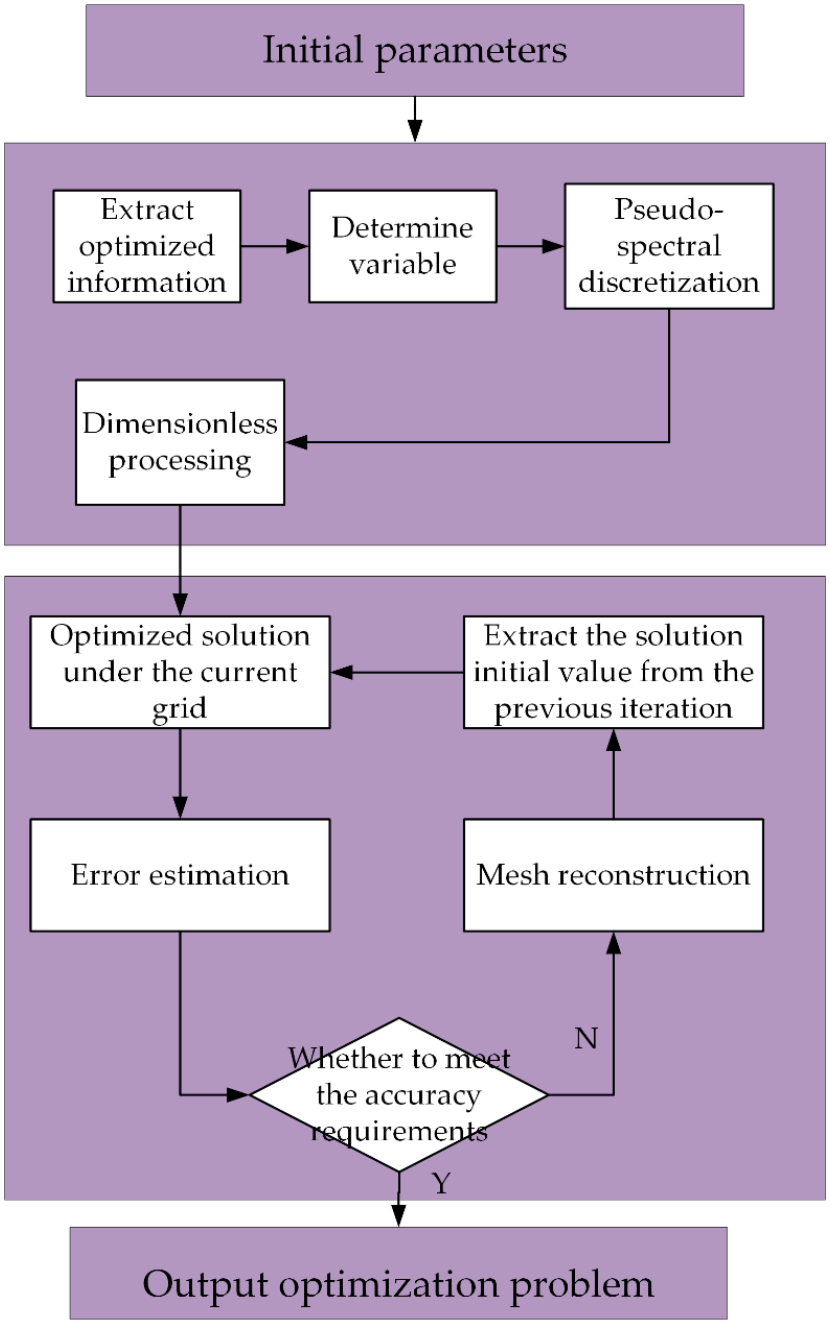

Figure 4. Algorithm flowchart.

GPM is used to optimize the cost functions of Equations (34)–(36) in three different situations. The results are shown in Figure 5.

When the cost function is a Lagrange function, the projectile flight state parameters are smooth and VCEC, LCEC, and roll control command are stable, which shows that the trajectory optimization model of the two-dimensional trajectory correction projectile based on the CEC is effective and feasible. When the CEC (Mayer function) is not taken into account, the trajectory obtained by the optimization calculation can accurately hit the target, as shown in Table 5. However, during the correction process, the change in the trajectory deflection angle fluctuates greatly, causing the lateral distance of the trajectory to swing from side to side (viewed from the tail of the bullet), as shown in Figure 5b; the output values of VCEC and LCEC change quickly, as shown in Figure 5f,g, which leads to a faster rate of change of the roll control command, as shown in Figure 5h. In practice, the short

interval between the two-step roll control commands will make the steering gear in the correction components unable to respond, and the canard cannot effectively execute the control command, resulting in the inability to effectively correct the trajectory. After adding the CEC (composite function), the projectile can still accurately hit the target, the vibration phenomenon that appears in the trajectory lateral distance curve is eliminated, continuous and stable VCEC and LCEC are output, and a smooth trajectory lateral distance and stable canard roll control command are obtained.

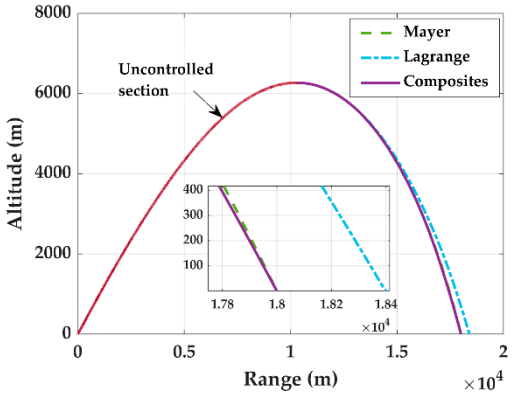

(**a**) Altitude vs. range

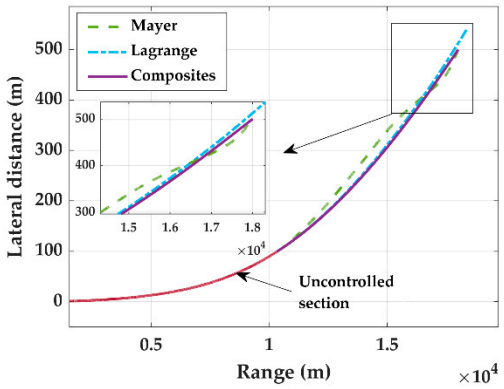

(**b**) Lateral distance vs. range

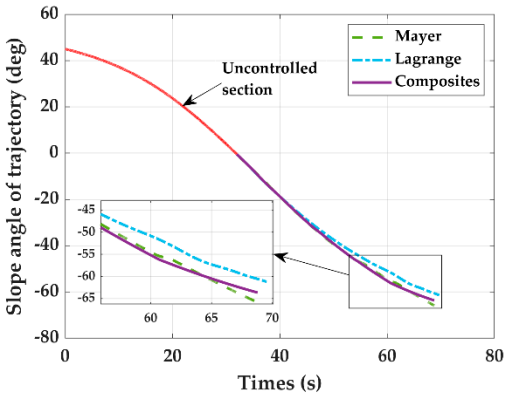

(**c**) Slope angle of trajectory vs. time

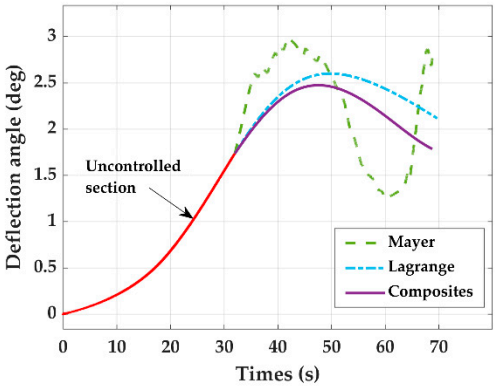

(**d**) Deflection angle vs. time

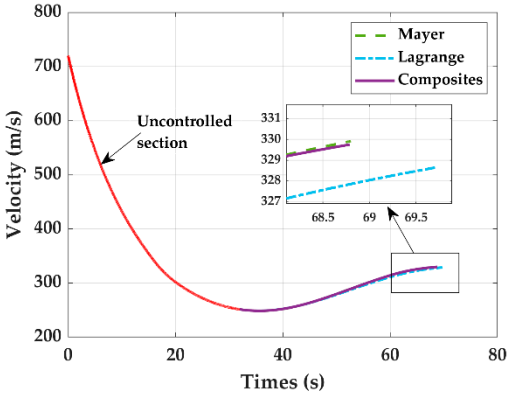

(**e**) Velocity vs. time

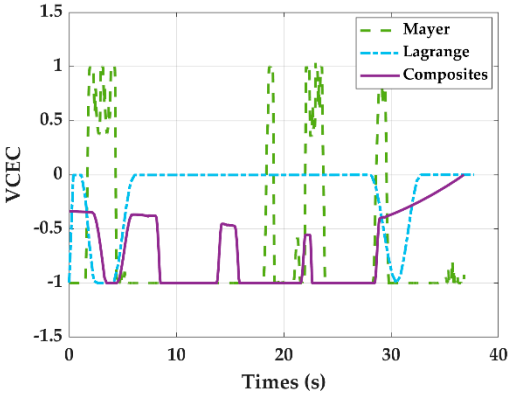

(**f**) VCEC vs. time

Figure 5. *Cont.*

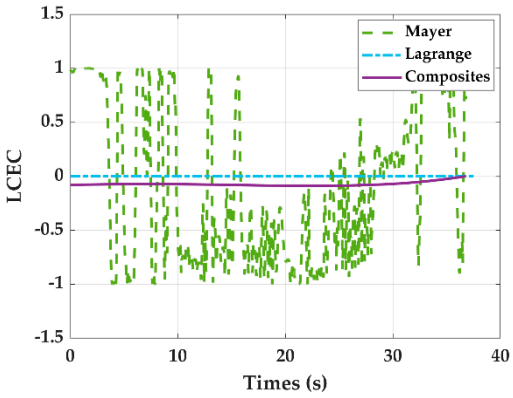

(**g**) LCEC vs. time

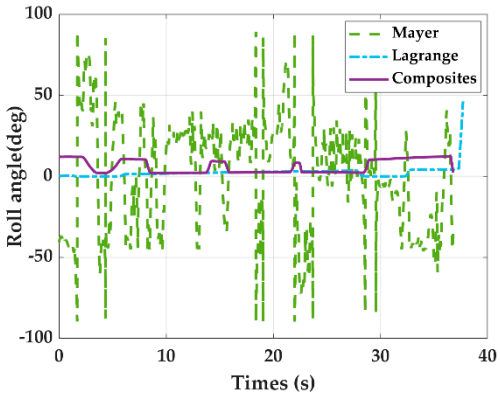

(**h**) Roll angle vs. time

Figure 5. Trajectory optimization results.

Table 5. Impact parameters with some constant CEC.

Cost Function	Velocity, m/s	Impact Angle, deg	Deflection Angle, deg	Impact Point
Mayer	329.9	65.87	2.77	(17,999, 500)
Lagrange	328.65	61.35	2.1	(18,397, 542)
Composite	329.78	63.98	1.8	(18,000, 500)

4.2. Trajectory Optimization for Different Targets

In this section, the composite function is used as the cost function to verify the applicability of the CEC and study the impact of the CEC on projectile shooting accuracy.

As is shown in Figure 6, different trajectories can be optimized by the CEC to deal with different combat tasks, and a stable optimized trajectory without trajectory swing and severe vibration of roll control command is obtained. As shown in Figure 6f–h, the VCEC and LCEC curves of different trajectories are stable, and the roll control command does not change drastically. The results not only meet the requirements of shooting accuracy but also output stable control command. The research in this section further verifies the feasibility of the proposed CEC model.

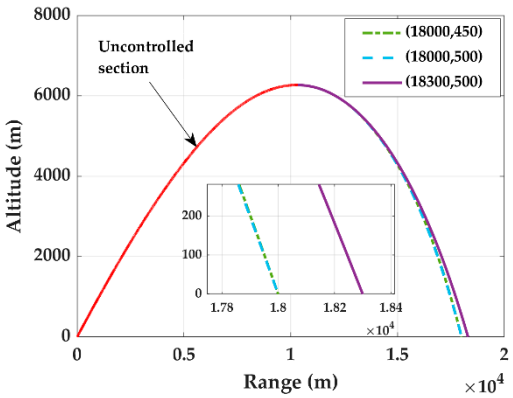

(**a**) Altitude vs. range

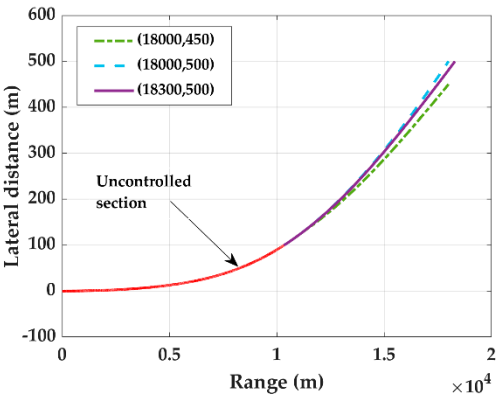

(**b**) Lateral distance vs. range

Figure 6. *Cont.*

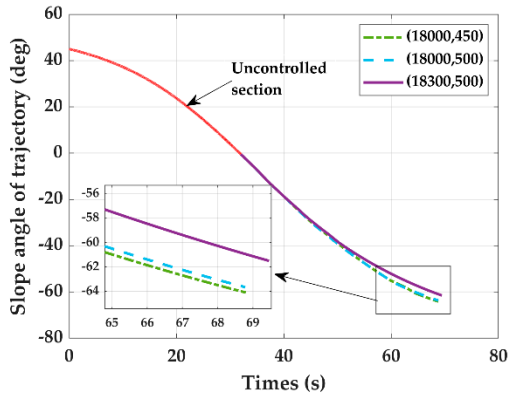

(**c**) Slope angle of trajectory vs. time

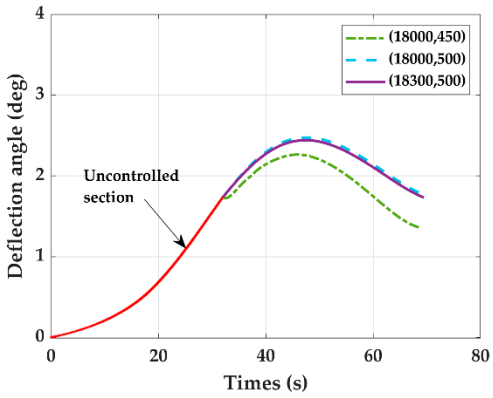

(**d**) Deflection angle vs. time

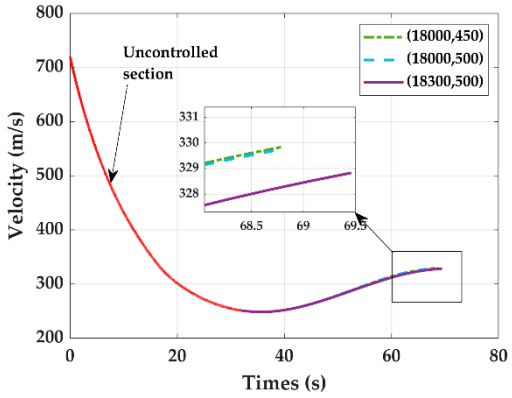

(**e**) Velocity vs. time

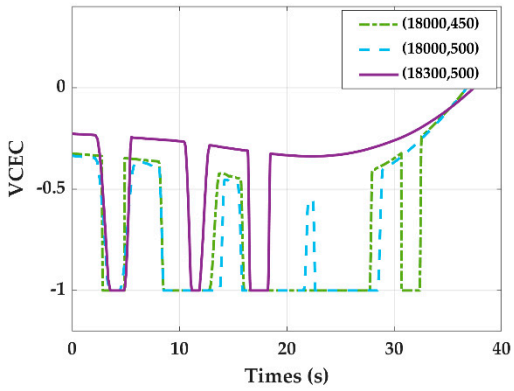

(**f**) VCEC vs. time

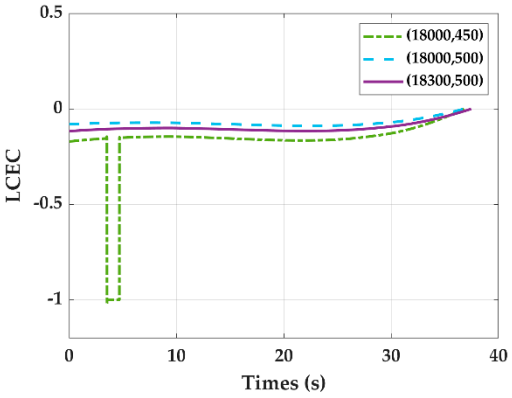

(**g**) LCEC vs. time

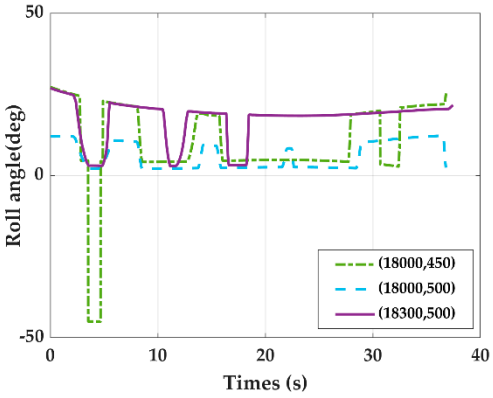

(**h**) Roll angle vs. time

Figure 6. Trajectory optimization of different impact points.

5. Design of Canard Geometry Based on CEC

5.1. Canard Wingspan Design

The control force and control moment of the two-dimensional trajectory correction projectile are provided by the canard. The canard is mounted on the nose of the projectile, and the trajectory of the projectile is corrected by the rolling effect. When the airflow passes through the two-dimensional trajectory correction projectile, the up–down wash effect will occur at the edge of the canard, resulting in relative interference between the canard and the projectile body. This interference has a great impact on the moment coefficient, thus affecting the aerodynamic layout of the projectile. In this section, the CEC will be combined into the optimization of the canard geometry's design.

Considering the mutual interference between the canard and the projectile, Equation (13) can be rewritten as

$$\begin{cases} \alpha = -\frac{c_{M_\delta}}{c_{lM_\alpha}}\delta_z \cos\gamma_f \\ \beta = -\frac{c_{M_\delta}}{c_{lM_\alpha}}\delta_z \sin\gamma_f \end{cases} \tag{37}$$

where c_{lM_δ} is the control moment coefficient considering geometric parameters; it consists of two parts: the control moment under the condition of angle of attack and the control moment under the condition of canard deflection, as shown in Equation (38).

$$c_{lM_\delta} = (K_\alpha c_{N_\delta}\alpha + K_{\delta_z} c_{N_\delta}\delta_z \cos\gamma_f) \cdot \frac{L_W}{D} \tag{38}$$

where K_α is the interference coefficient at the angle of attack, K_{δ_z} is the interference coefficient in the case of canard deflection; L_W is the distance from the center of the canard to the center of mass.

$$\begin{cases} K_\alpha = (1+K_s)^2 \\ K_{\delta_z} = \frac{1}{5}[(2+K_s)^2+1] \end{cases} \tag{39}$$

where K_s is the ratio of the diameter of the projectile body at the installation position of the canard to the wingspan; $K_s = D/l$, D is the canard installation position projectile diameter, l is the wingspan.

Let $c_{l\alpha\delta} = -\frac{c_{M_\delta}}{c_{lM_\alpha}}$, and then Equation (37) can be rewritten as:

$$\begin{cases} \alpha = c_{l\alpha\delta}\delta_{zy} \\ \beta = c_{l\alpha\delta}\delta_{zz} \end{cases} \tag{40}$$

Substituting Equation (40) into Equations (22) and (23), we get:

$$\begin{cases} \xi_Y = \text{sign}(\delta_{zy})\frac{2\sqrt{K_{lA}K_B}\delta_{zy}}{K_B+K_{lA}\delta_{zy}^2} \\ \xi_Z = \text{sign}(\delta_{zz})\frac{2\sqrt{K_{lA}K_B}\delta_{zz}}{K_B+K_{lA}\delta_{zz}^2} \end{cases} \tag{41}$$

The relationship between VCEC and LCEC and canard wingspan is shown in Equation (41). The smaller the canard wingspan is, the smaller the VCEC and LCEC are, and vice versa. Next, take $K_s = 0.2 \sim 0.6$ and use Equation (36) as the cost function for trajectory optimization calculation. The results are shown in Figure 7.

The simulation results are shown in Figure 7. When $K_s = 0.2$, the canard has the largest wingspan. A larger wingspan can provide greater control force and moment but increase VCEC and LCEC relatively, which is inconsistent with the conclusion that a smaller VCEC and LCEC are conducive to trajectory optimization in Section III. When the trajectory is corrected, a larger wingspan will lead to a larger overload, which will affect the flight stability of the projectile and cause the vibration and mutation of the trajectory deflection curve. When $K_s = 0.6$, the wingspan is the smallest. Because the wingspan is too small, the control force and moment provided are insufficient, and the deflection angle, VCEC, LCEC, and roll angle command curves have vibration and sudden change. When $K_s = 0.4$, the state parameter curve of the projectile flying is the smoothest and the roll control command is the most stable, indicating the best canard wingspan. Hence, we can refer to the values of VCEC and LCEC to obtain the best wingspan for a two-dimensional trajectory correction projectile.

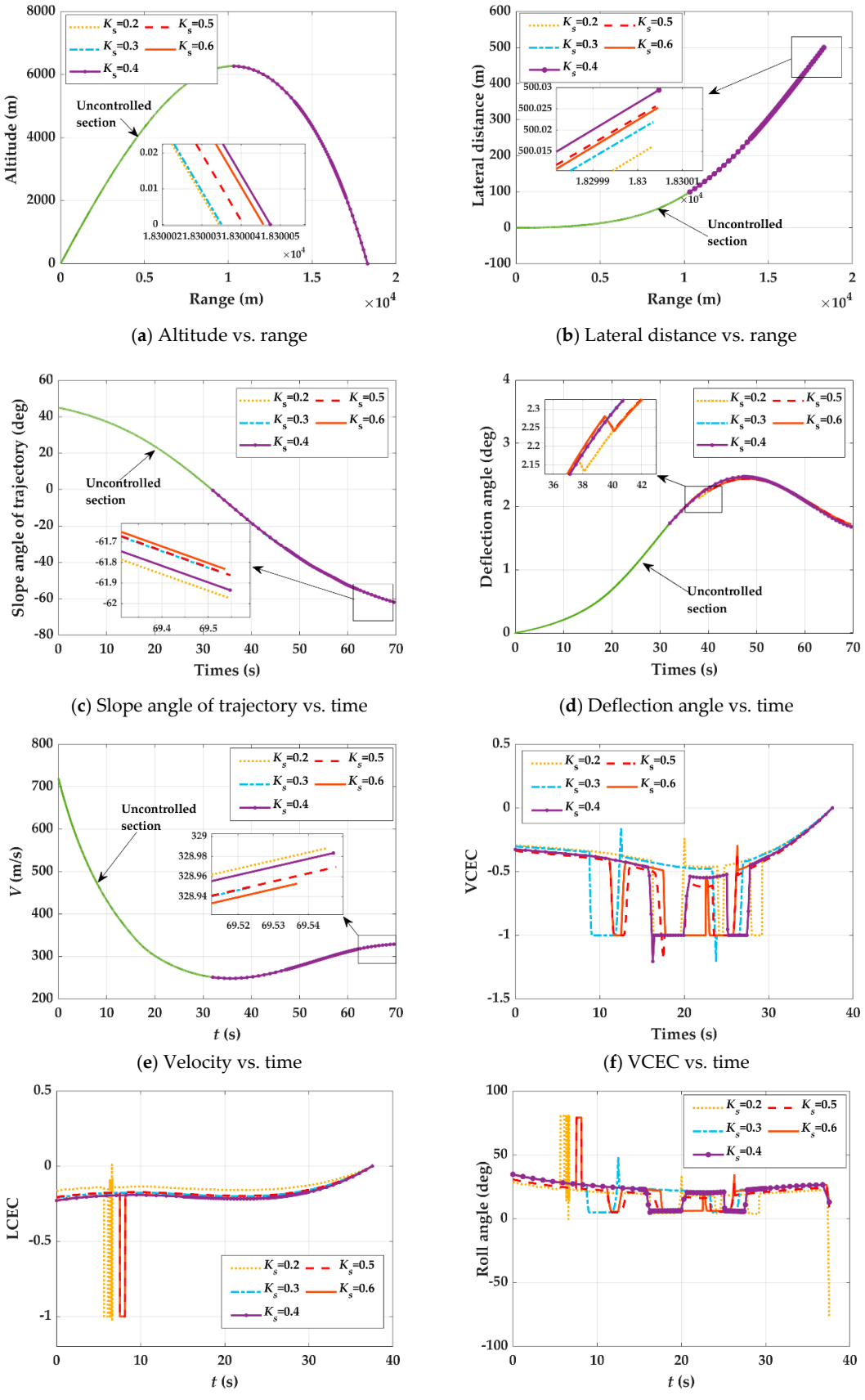

(**a**) Altitude vs. range

(**b**) Lateral distance vs. range

(**c**) Slope angle of trajectory vs. time

(**d**) Deflection angle vs. time

(**e**) Velocity vs. time

(**f**) VCEC vs. time

(**g**) LCEC vs. time

(**h**) Roll angle vs. time

Figure 7. Trajectory optimization of different aspect ratios.

5.2. Canard Shape Design

The equation of the exposed wing's aspect ratio of two-dimensional trajectory correction projectile:

$$\lambda_{wl} = \lambda \frac{1 - K_s}{1 - \frac{\eta - 1}{\eta + 1} K_s} \tag{42}$$

where λ is the aspect ratio of the canards; λ_{wl} is the aspect ratio of the exposed canards; η is the root tip ratio.

$$K_s = \frac{1 - K_\lambda}{1 - K_\lambda K_\eta} \tag{43}$$

where $K_\lambda = \lambda_{wl}/\lambda$, $K_\eta = (\eta - 1)/(\eta + 1)$.

Different shapes of canards have different root tip ratios. When the shape of the canard is rectangular, then $K_\eta = 0$, and the K_s of the rectangular canard $K_{\text{Rect}} = 1 - K_\lambda$. When the shape of the canard is trapezoidal, then $\eta < 1$ and $K_\eta < 0$, $(1 - K_\lambda K_\eta) > 1$, and it can be seen that $K_{\text{Trape}} < K_{\text{Rect}}$. Hence, when the K_λ is the same, if the trapezoidal canard projectile is installed, the CEC is smaller, and the trajectory optimization result should be better.

The results show that the two shapes of canards can control the projectile to accurately hit the target. As shown in Figure 8d–h, the optimized projectiles with trapezoidal canards installed have smoother flight parameters, smaller VCEC and LCEC, and more stable roll control command, which proves that the results are consistent with the above theoretical analysis. Therefore, when the structural parameters are the same, installing the trapezoidal canard can make the pressure center closer to the nose of the projectile so that the control effect of the canard is better.

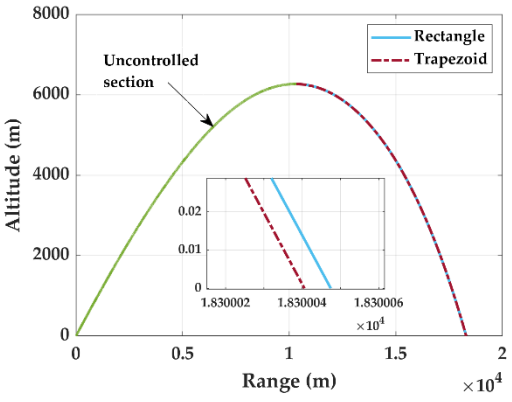

(**a**) Altitude vs. range

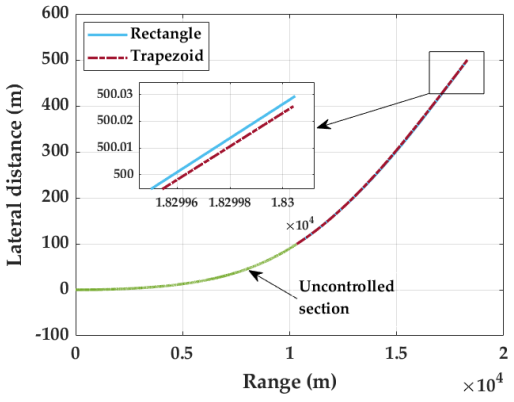

(**b**) Lateral distance vs. range

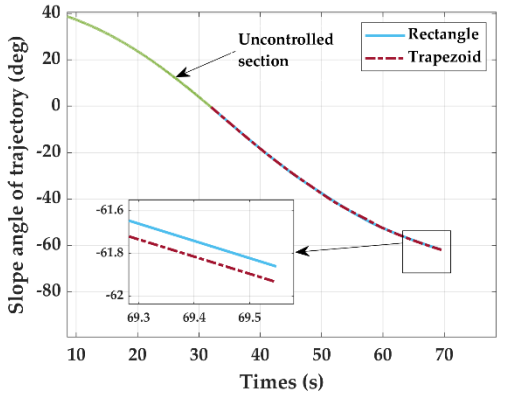

(**c**) Slope angle of trajectory vs. time

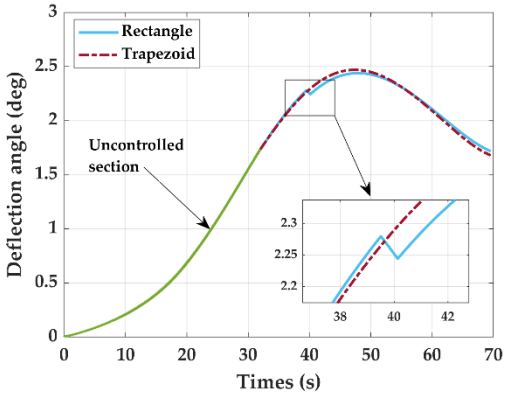

(**d**) Deflection angle vs. time

Figure 8. *Cont.*

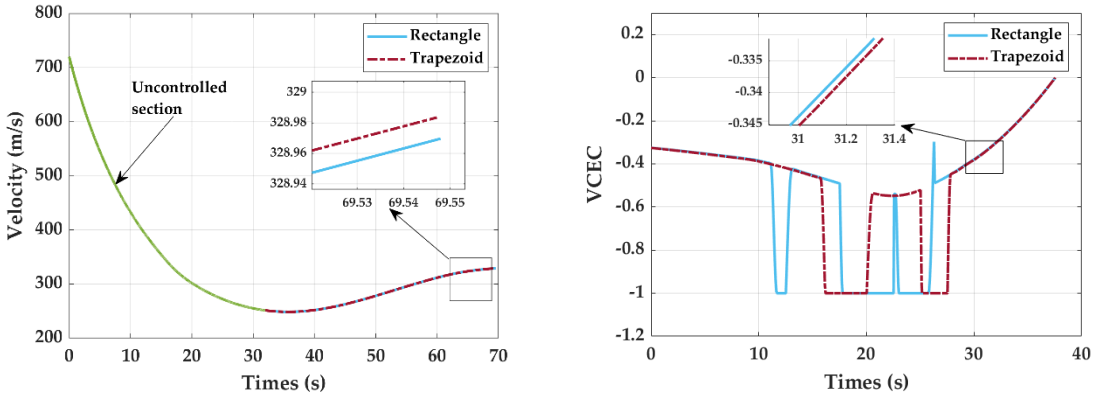

(**e**) Velocity vs. time (**f**) VCEC vs. time

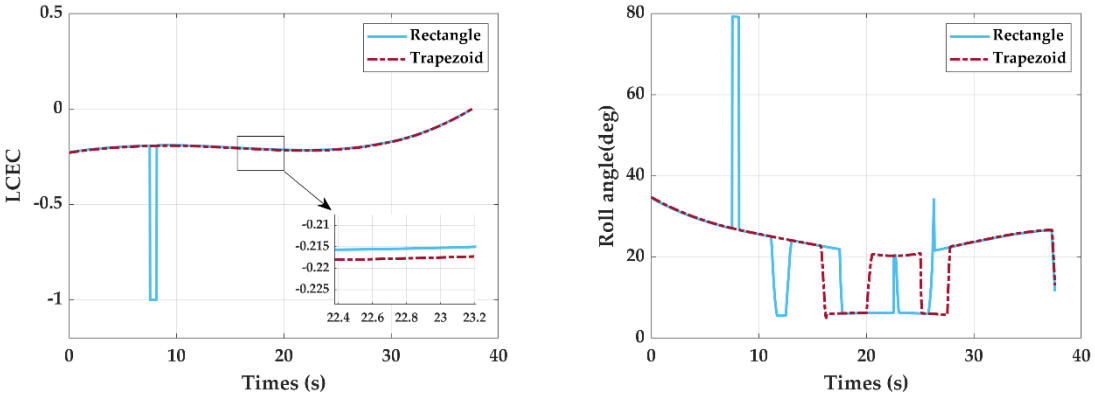

(**g**) LCEC vs. time (**h**) Roll angle vs. time

Figure 8. Trajectory optimization of different canards.

6. Conclusions

Based on the lift-to-drag ratio, the novel concept of the correction efficiency coefficient was proposed and applied on the trajectory optimization of the two-dimensional trajectory correction projectile in this paper. The theoretical analysis and simulation indicate that, the smaller the value of the CEC is, the stronger the correction ability is. In a constraint-free environment, a CEC can effectively correct the trajectory of a two-dimensional trajectory correction projectile and reflect the pattern of the canard's roll angle changes. After the CEC (composite function) is added, the projectile can still accurately hit the target, the vibration phenomenon that appears in the trajectory lateral distance curve is eliminated, and a stable canard roll control command is obtained. Based on the CEC, the two-dimensional trajectory correction projectile canard geometry is optimized, and the influences different wingspans and shapes have on the trajectory optimization are studied. When the canard diameter aspect ratio is 0.4, the projectile flight status is more stable and the roll control command is better. When the canard is trapezoidal, the CEC is smaller, the trajectory is more stable, and the output roll control command stability is better. In future work, the angular motion law of a two-dimensional trajectory correction projectile can also be analyzed in combination with the CEC, and the geometric mechanism parameters of the canard can be further optimized (such as canard rudder sweep angle, chord length, installation position, etc.). The research results of this paper can provide a certain reference for the trajectory design of the two-dimensional trajectory correction projectile and the optimization of the canard geometry.

Author Contributions: Conceptualization, D.Z.; methodology, D.Z.; software, D.Z. and Q.G.; validation, D.Z.; formal analysis, D.Z.; investigation, D.Z. and Q.N.; resources, D.Z. and Z.J.; writing—original draft preparation, D.Z.; writing—review and editing, D.Z.; supervision, J.Z. and Z.J.; project

administration, J.Z.; funding acquisition, J.Z. All authors have read and agreed to the published version of the manuscript.

Funding: This research is not funded by any external funds.

Conflicts of Interest: The authors declare no conflict of interest.

References

1. Shen, Q.; Li, D.; Ji, X. *Technology of Trajectory Correction Fuze*; National Defense Industry Press: Beijing, China, 2016; pp. 1–10.
2. Norris, J.; Hameed, A.; Economou, J.; Parker, S. A Review of Dual-spin Projectile Stability. *Def. Technol.* **2020**, *16*, 1–9. [CrossRef]
3. Costello, M.F. Modeling and Simulation of a Differential Roll Projectile. In *Proceedings of the 1998 AIAA Modeling and Simulation Technologies Conference, Boston, MA, USA, 10–12 August 1998*; AIAA: Reston, VA, USA, 1998; pp. 490–499.
4. Wernert, P.; Theodoulis, S. Modelling and Stability Analysis for a Class of 155 mm Spin-stabilized Projectiles with Course Correction Fuse (CCF). In Proceedings of the AIAA Atmospheric Flight Mechanics Conference, Portland, OR, USA, 8–11 August 2011; pp. 1–14.
5. Chang, S. Dynamic Response to Canard Control and Gravity for a Dual-Spin Projectile. *J. Spacecr. Rocket.* **2016**, *53*, 558–566. [CrossRef]
6. Brauer, G.L.; Cornick, D.E.; Stevenson, R. *Capabilities and Applications of the Program to Optimize and Simulate Trajectories*; NASA-CR-2770; NASA: Springfield, VA, USA, 1977.
7. Darby, C.L.; Hager, W.W.; Rao, A.V. Direct trajectory optimization using a variable low-order adaptive pseudo-spectral method. *J. Spacecr. Rocket.* **2011**, *48*, 433–445. [CrossRef]
8. Huo, P.; Shi, K.; Yuan, W. Research on Trajectory Controlled Optimization for Trajectory Correction Fuze Using Maximum Principle. *Acta Armamentarii* **2007**, *28*, 301–304.
9. Vormer, F.J.; Mulder, M.; van Paassen, M.M.; Mulder, J.A. Optimization of Flexible Approach Trajectories Using a Genetic Algorithm. *J. Aircr.* **2006**, *43*, 941–952. [CrossRef]
10. Kitayama, S.; Yamazaki, K.; Arakawa, M. Adaptive Range Particle Swarm Optimization. In Proceedings of the 11th AIAA/ISSMO Multidisciplinary Analysis and Optimization Conference, Portsmouth, VA, USA, 6–8 September 2006; pp. 1–10.
11. Berguin, S.H.; Dunn, A.K.; Sonnenburg, C.; Allison, D.L. Surrogate-Based Trajectory Optimization Using Gradient-Enhanced Neural Networks. In Proceedings of the AIAA Aviation 2021 Forum, Virtual, 2–6 August 2021.
12. Costello, M. Range Optimization of a Fin Stabilized Projectile. In Proceedings of the 22nd Atmospheric Flight Mechanics Conference, New Orleans, LA, USA, 11–19 August 1997; pp. 695–699.
13. Liu, C.; Zhang, C. Multi-stage Trajectory Optimization of Tactical Two-stage Booster Rocket Based on Gauss Pseudo-spectral Method. *Acta Armamentarii* **2019**, *40*, 292–302.
14. Chen, Q.; Wang, Z.; Chang, S.; Fu, J. Multiphase Trajectory Optimization for Gun-Launched Glide Guided Projectiles. *J. Aerosp. Eng.* **2015**, *6*, 995–1010. [CrossRef]
15. Xu, Q.; Chang, S.; Wang, Z. Composite-Efficiency-Factor-Based Trajectory Optimization for Gliding Guided Projectiles. *J. Spacecr. Rocket.* **2018**, *55*, 66–76. [CrossRef]
16. Burchett, B.T. A Gauss Pseudo-spectral Collocation for Rapid Trajectory Prediction and Guidance. In Proceedings of the AIAA Atmospheric Flight Mechanics Conference, Grapevine, TX, USA, 9–13 January 2017; pp. 1–20.
17. Yao, J.; Wang, X.; Wang, X.B. Solution for Trajectory Correction Optimization Based on Generalized Work Principle. In Proceedings of the 2010 5th IEEE Conference on Industrial Electronics and Applications, Taichung, Taiwan, 15–17 June 2010; pp. 232–236.
18. Wu, Y.; Deng, J.; Li, L.; Su, X.; Lin, L. A hybrid particle swarm optimization-gauss pseudo method for reentry trajectory optimization of hypersonic vehicle with navigation information model. *Aerosp. Sci. Technol.* **2021**, *118*, 107046. [CrossRef]
19. Arnoult, G.; Zeidler, M.; Garnier, E. Control Surface Geometry Surrogate-Based Optimization for Spin-Stabilized Projectile Course Correction. *AIAA J.* **2020**, *58*, 550–560. [CrossRef]
20. Zhou, W.; Zhang, J.; Ni, Q.; Hao, Y.; Liang, Y. Research on Parametric Modeling Optimization of Trajectory Correction Projectile Based on FVM. *Teh. Vjesn. Tech. Gaz.* **2021**, *28*, 907–913.
21. Wang, Z. Optimal trajectories and normal load analysis of hypersonic glide vehicles via convex optimization. *Aerosp. Sci. Technol.* **2019**, *87*, 357–368. [CrossRef]
22. Kwon, H.-H.; Hong, S.-M.; Kim, G.-H.; Kim, Y.-H. Mid-course Trajectory Optimization for Boost-Glide Missiles Based on Convex Programming. *J. Korean Soc. Aeronaut. Space Sci.* **2021**, *49*, 21–30.
23. Laad, D.; Elango, P.; Mohan, R. Fourier Pseudo-spectral Method for Trajectory Optimization with Stability Requirements. *J. Guid. Control. Dyn.* **2020**, *43*, 2073–2090. [CrossRef]
24. Elsisi, M. Optimal design of nonlinear model predictive controller based on new modified multitracker optimization algorithm. *Int. J. Intell. Syst.* **2020**, *35*, 1857–1878. [CrossRef]
25. Elsisi, M.; Ebrahim, M.A. Optimal design of low computational burden model predictive control based on SSDA towards autonomous vehicle under vision dynamics. *Int. J. Intell. Syst.* **2021**, *36*, 6968–6987. [CrossRef]
26. Elsisi, M. Improved grey wolf optimizer based on opposition and quasi learning approaches for optimization: Case study autonomous vehicle including vision system. *Artif. Intell. Rev.* **2022**. [CrossRef]
27. Han, Z.P. *Exterior Ballistics of Shells and Rockets*, 2nd ed.; Beijing University of Technology Press: Beijing, China, 2008; pp. 179–180.

28. Benson, D.A. *A Gauss Pseudo-Spectral Transcription for Optimal Control*; Massachusetts Institute of Technology: Cambridge, MA, USA, 2005.
29. Rao, A.V.; Benson, D.; Darby, C.L.; Mahon, B.; Francolin, C.; Patterson, M.; Sanders, I.; Huntington, G.T. *User's Manual for GPOPS Version 5.0: A MATLAB Software for Solving Multiple-Phase Optimal Control Problems Using hp-Adaptive Pseudo-spectral Methods*; University of Florida: Gainesville, FL, USA, 2011.
30. Gill, P.E.; Murray, W.; Saunders, M.A. SNOPT: An SQP Algorithm for Large-Scale Constrained Optimization. *SIAM J. Optim.* **2002**, *12*, 979–1006. [CrossRef]